Surpporting Information

H- and J-Aggregation Inspiring Efficient Solar Conversion

Qiaoqiao Zhao ‡[a,b], Hanjian Lai ‡[a], Hui Chen [a], Heng Li [a], Feng He *[a,c]

[a.] *Shenzhen Grubbs Institute and Department of Chemistry, Southern University of Science and Technology, Shenzhen 518055, China, E-mail: hef@sustech.edu.cn (F.H.).*

[b.] *State Key Laboratory of Biobased Material and Green Papermaking, Qilu University of Technology, Shandong Academy of Sciences, Jinan 250353, China.*

[c.] *Guangdong Provincial Key Laboratory of Catalysis, Southern University of Science and Technology, Shenzhen 518055, China.*

‡The authors contributed equally to this work.

Experimental Section

Device fabrication: Solar cells were fabricated with inverted structure ITO/ZnO/active layer/ MoO_x /Ag. The ITO substrates were ultrasonicated sequentially in detergent, deionized water, acetone and isopropyl alcohol and dried at 80 ℃ in vacuum oven, followed by UV-ozone treatment for 15 min to modify surface. ZnO, for electron injection, was spin-coated at 3000 rpm for 30 s onto the pre-treated ITO substrates from precursor solution, then heated at 200 ℃ for 20 min. Active layer was spin-coated onto ZnO from chloroform (CF) solution of totally 11 mg/ml PBDB-TF/BTIC-CF_3-m blend with 0.5% (v/v) 1,8-diiodooctane (DIO) or 1-chloronaphthalene (CN). The device was finished after 10 nm molybdenum oxide (MoO_x) buffer and 100 nm Ag electrode deposited by thermal evaporation through a defined shadow mask in a vacuum chamber with a pressure of approximately 8×10^{-5} Pa.

Characterization: The UV-Vis absorption spectra were recorded by an Agilent Cary 60 UV-Vis spectrophotometer. Grazing incident wide-angle X-ray scattering (GIWAXS) measurements were performed at the 8ID-E beamline at the Advanced Photon Source (APS), Argonne National Laboratory using x-rays with a wavelength of λ = 1.1385 Å and a beam size of 200 μm (h) and 20 μm (v). A 2-D PILATUS 1M-F detector was used to capture the scattering patterns and was situated at 208.7 mm from samples. The photoluminescence (PL) spectra were recorded by an Edinburgh FS5 spectrofluorometer. Atomic force microscopy (AFM) images were obtained using an Asylum Research AFM in AC mode under ambient conditions. Transmission electron microscopy (TEM) micrographs were obtained on a Hitachi HT7700 microscope operating at 80kV and equipped with an AMF-5016 charge-coupled device camera. Steady-state current-voltage (*J-V*) curves were measured by a Keithley 2400 source-measurement unit under AM 1.5 G spectrum from a solar simulator (Enlitech.Inc) calibrated by a silicon reference cell (Hamamatsu S1133 color, with KG-5 visible fiith). The the relationship of J_{sc} to the light intensity were measured by steady-state current-voltage measurement, the light intensity was modulated by neutral density filters (NDF) with different values of optical density (OD). The external quantum efficiency (EQE) was measured by a solar cells–photodetector responsibility measurement system (Enlitech. Inc). The mobility of electron and hole was tested by fitting the current-bias characteristics in dark utilizing a field-independent space charge limited current (SCLC) model following the Mott-Gurney law given by $J = \frac{9}{8}\varepsilon_0\varepsilon_r\mu\frac{V^2}{L^3}$. The device structures for hole-only and electron-only

device are ITO/PEDOT:PSS/active layer/MoO_3/Ag and ITO/ZnO active layer/Ca/Al, respectively.

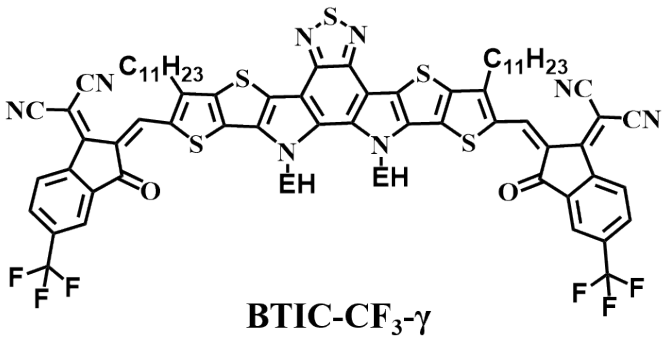

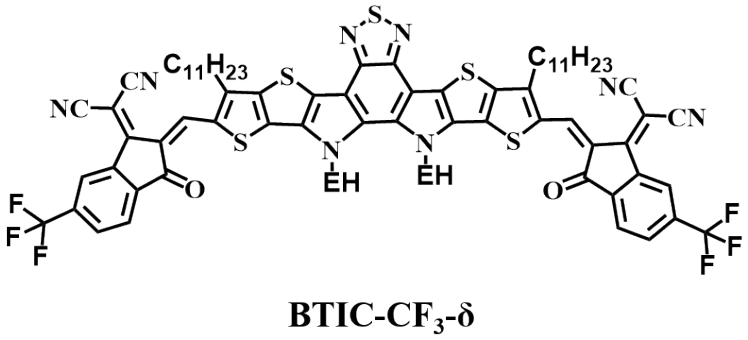

Figure S1. The chemical structures of BTIC-CF_3-γ and BTIC-CF_3-δ.

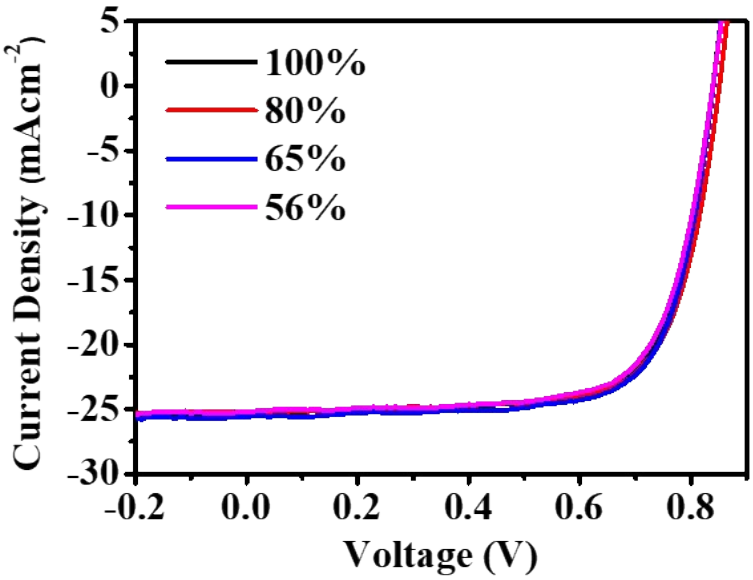

Figure S2. *J-V* curves of devices based on BTIC-CF_3-m with with different content of BTIC-CF_3-γ under 100 mW cm^{-2} light illumination.

Table S1. Photovoltaic parameters of devices based on BTIC-CF_3-m with different mixing ratios of BTIC-CF_3-γ and BTIC-CF_3-δ under 100 mW cm^{-2} light illumination.

BTIC-CF_3-γ	*Voc* (V)	*Jsc* (mA cm^{-2})	FF (%)	PCE (%)
100%	0.84	25.52	72.61	15.57
80%	0.85	25.54	72.69	15.78
65%	**0.84**	**25.89**	**72.89**	**15.85**
56%	0.84	25.50	71.80	15.38

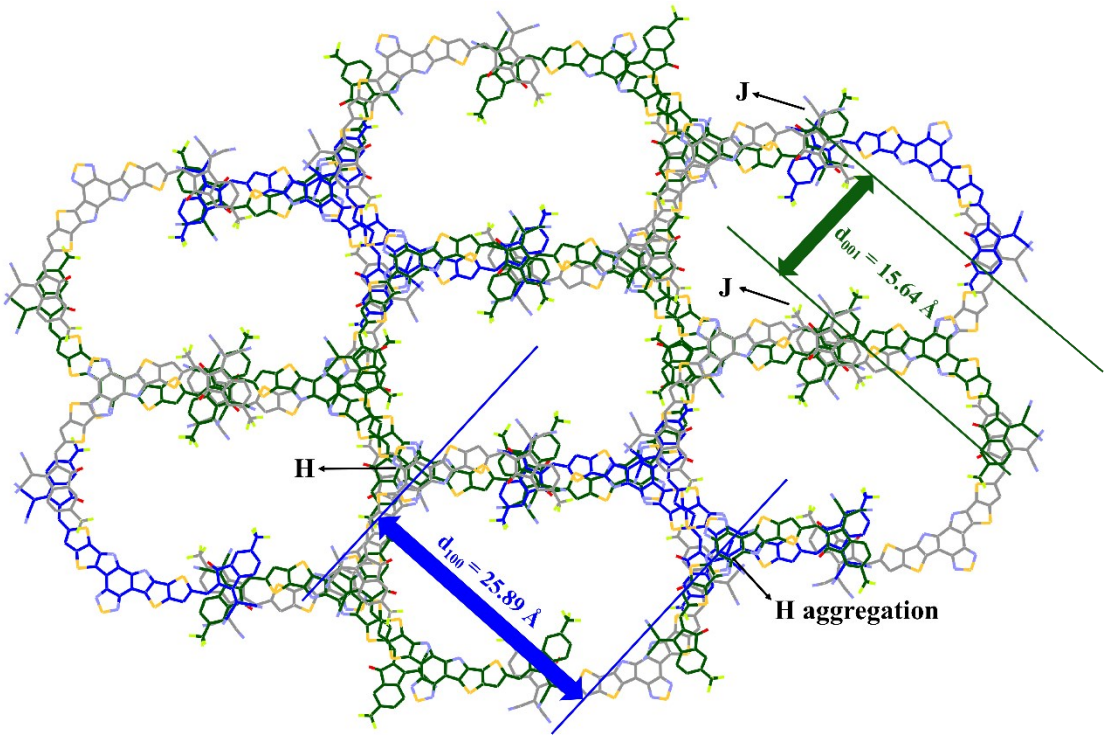

Figure S3. The single-crystal structure of BTIC-CF_3-γ.

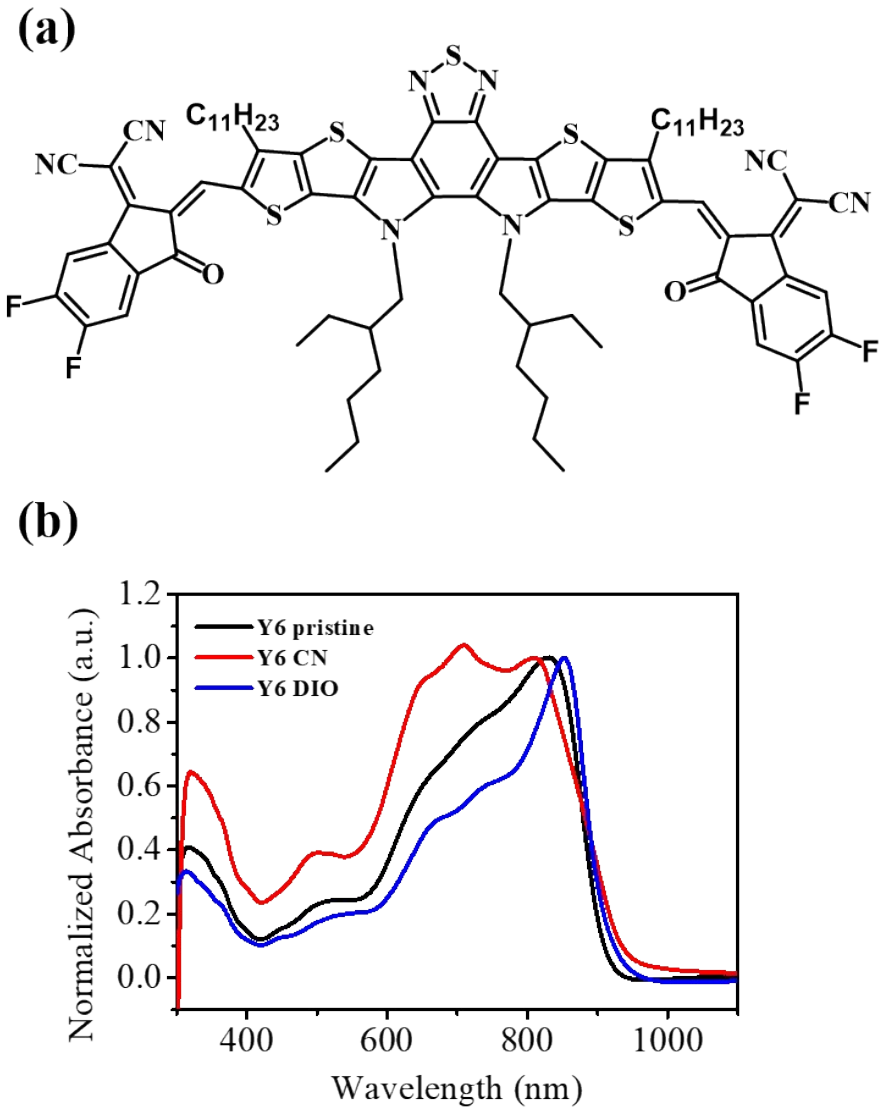

Figure S4. (a) The chemical structure and (b) absorbance of neat Y6 films without additive and with 1% CN or 1% DIO.

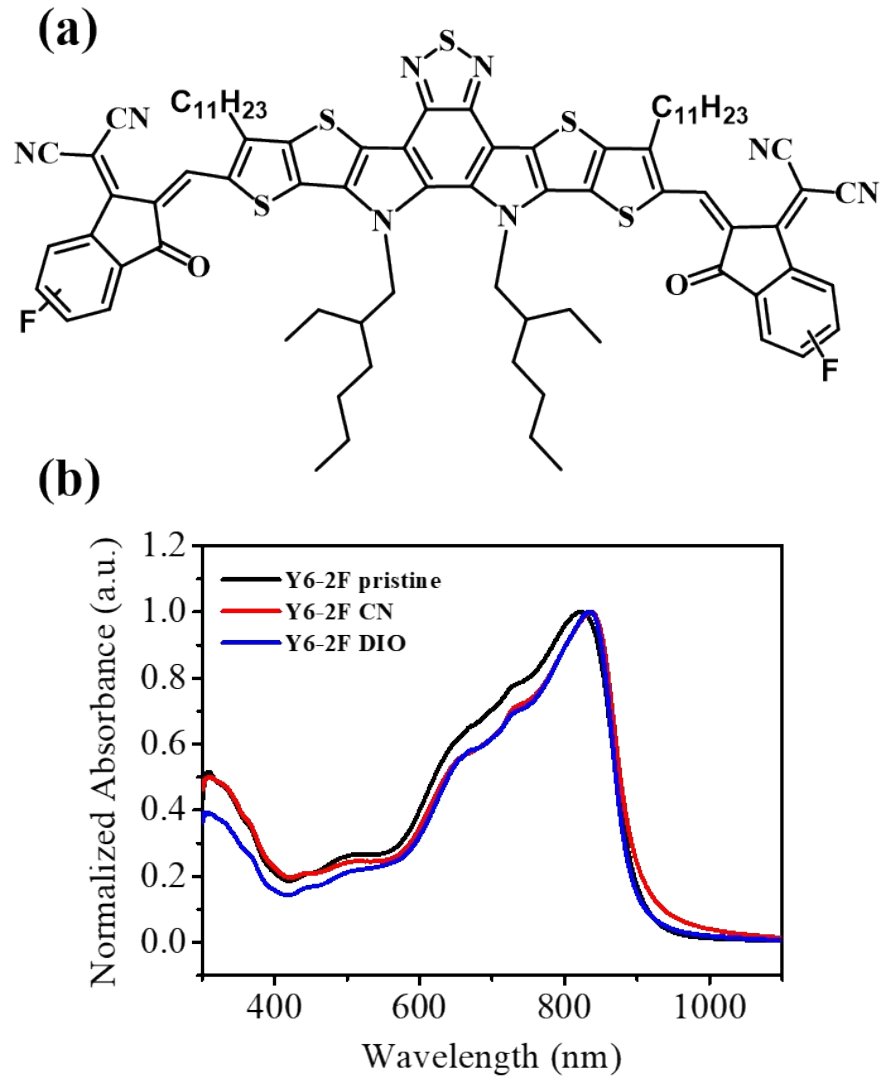

Figure S5. (a) The chemical structure and (b) absorbance of neat Y6-2F films without additive and with 1% CN or 1% DIO.

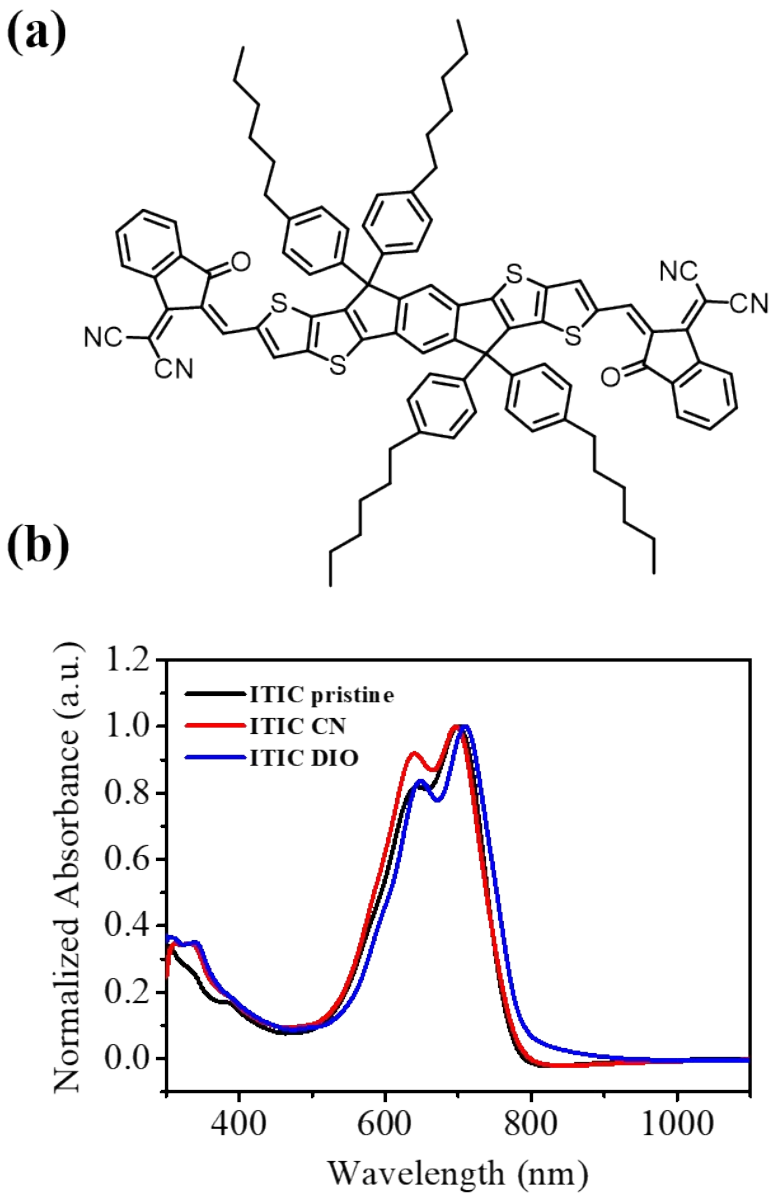

Figure S6. (a) The chemical structure and (b) absorbance of neat ITIC films without additive and with 1% CN or 1% DIO.

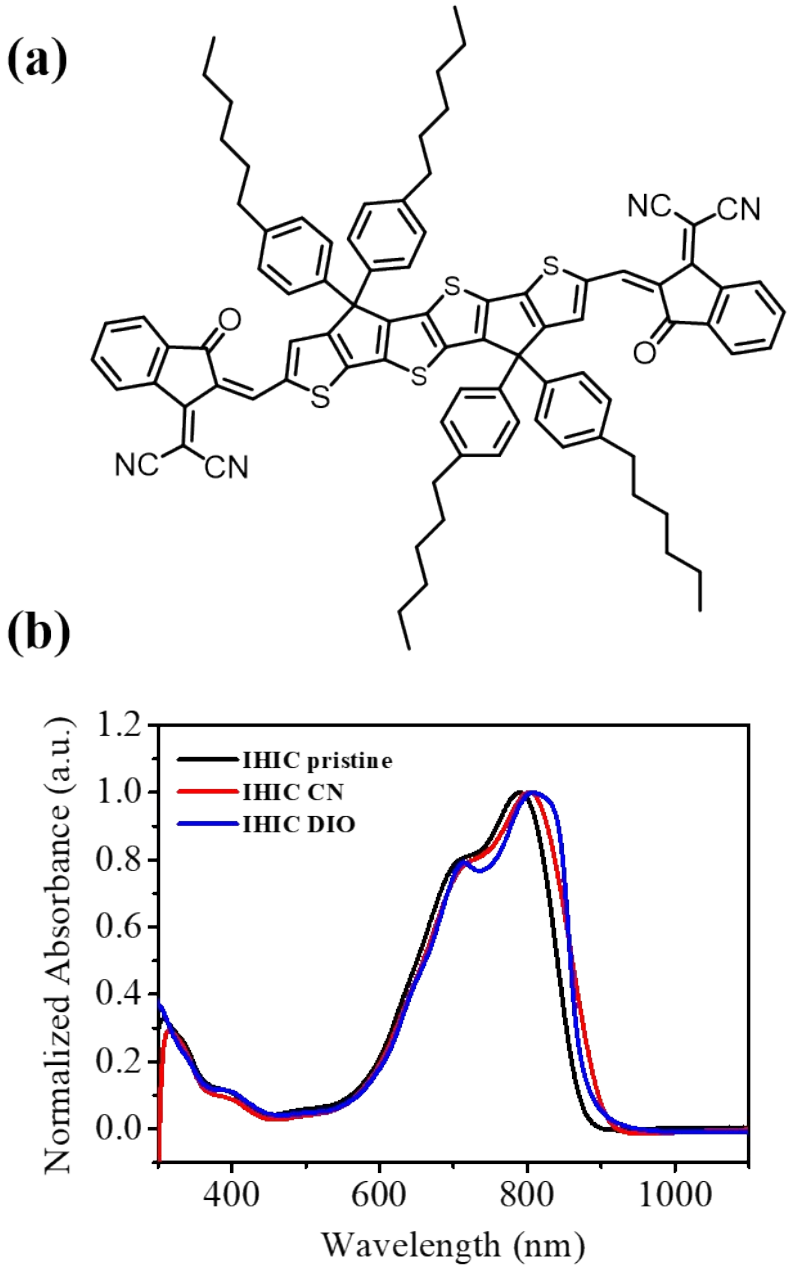

Figure S7. (a) The chemical structure and (b) absorbance of neat IHIC films without additive and with 1% CN or 1% DIO.

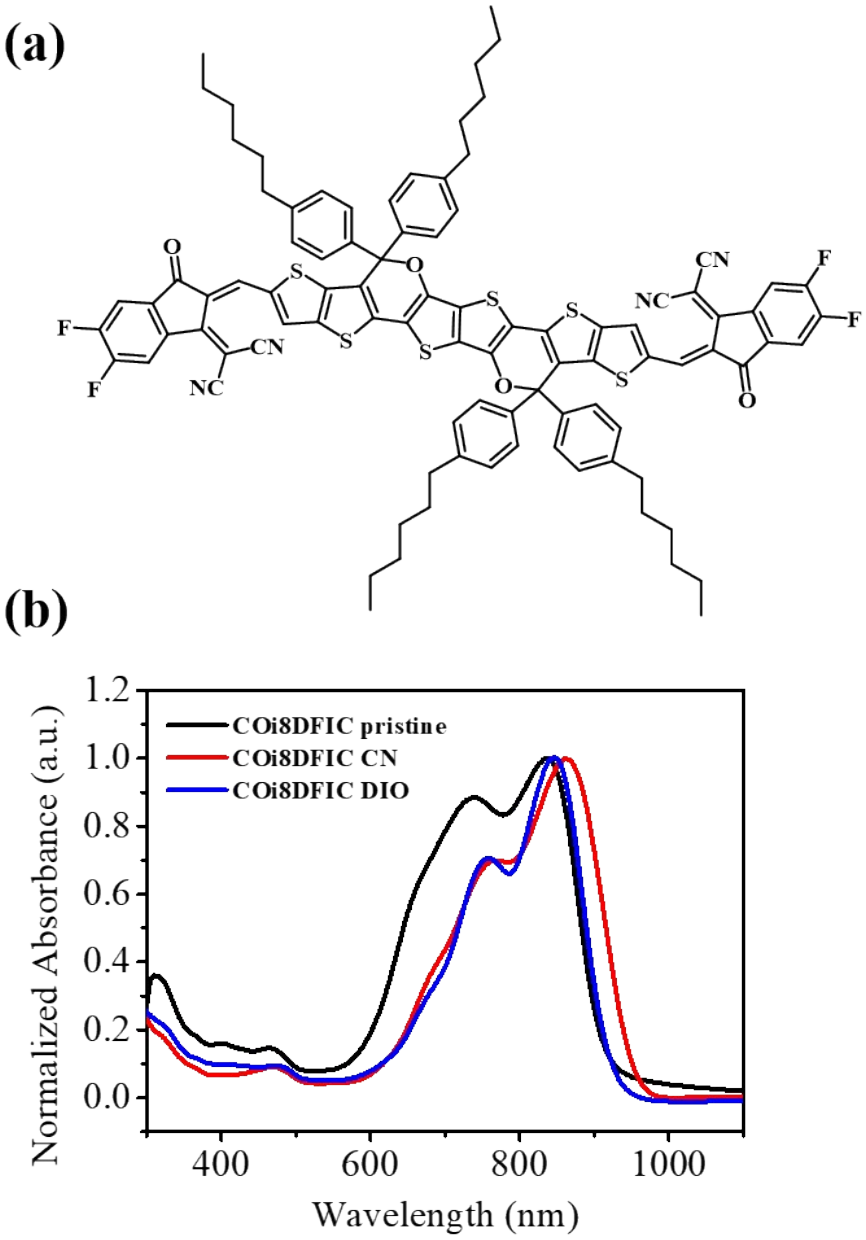

Figure S8. (a) The chemical structure and (b) absorbance of neat COi8DFIC films without additive and with 1% CN or 1% DIO.

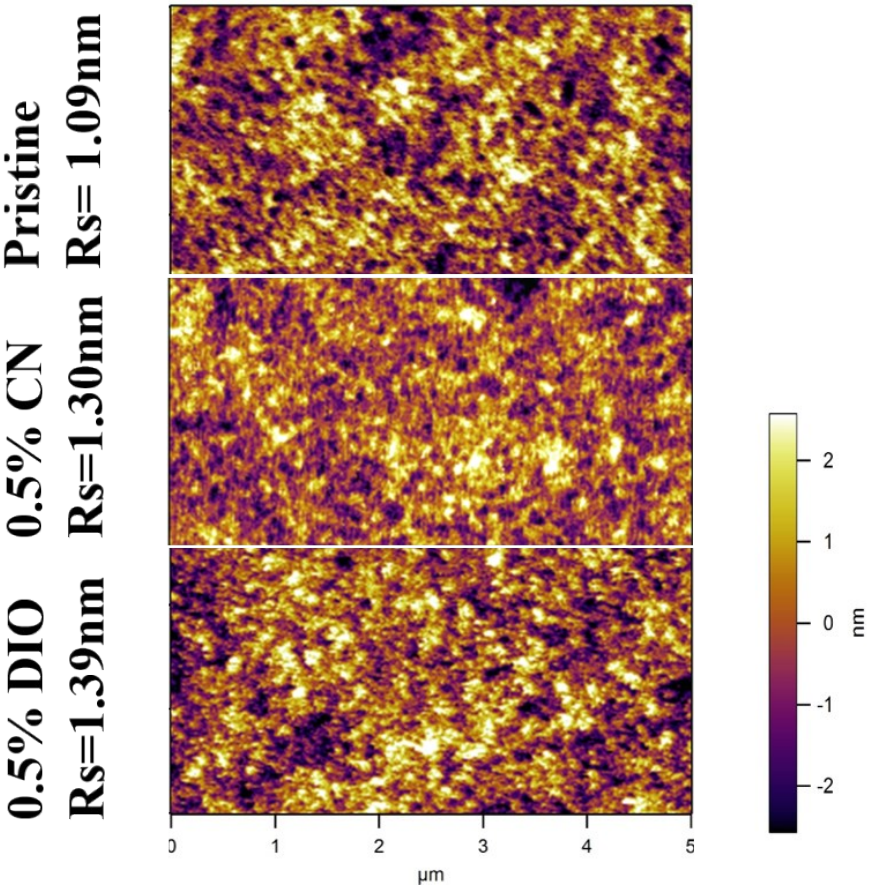

Figure S9. The AFM images of PBDB-TF:BTIC-CF_3-m blend films without additive or with 0.5% CN/DIO.

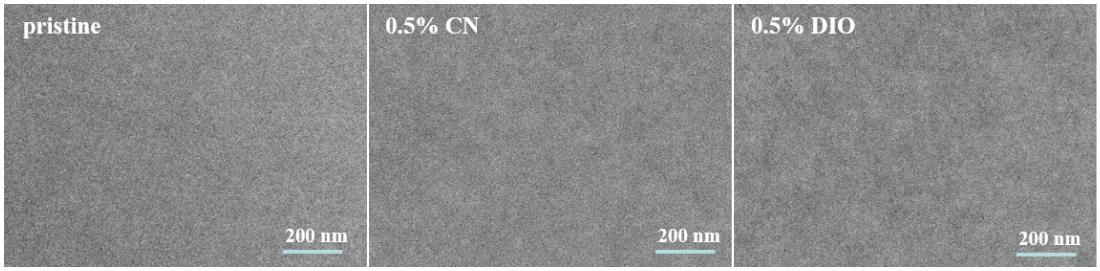

Figure S10. The TEM images of PBDB-TF:BTIC-CF_3-m blend films without additive or with 0.5% CN/DIO.

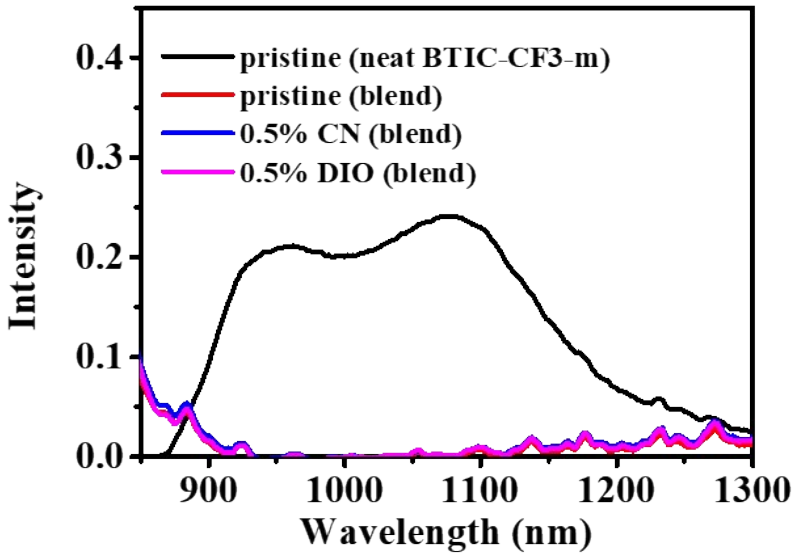

Figure S11. The PL profiles of pristine neat BTIC-CF_3-m film or PBDB-TF: BTIC-CF_3-m blend films without additive or with 0.5% CN/DIO.

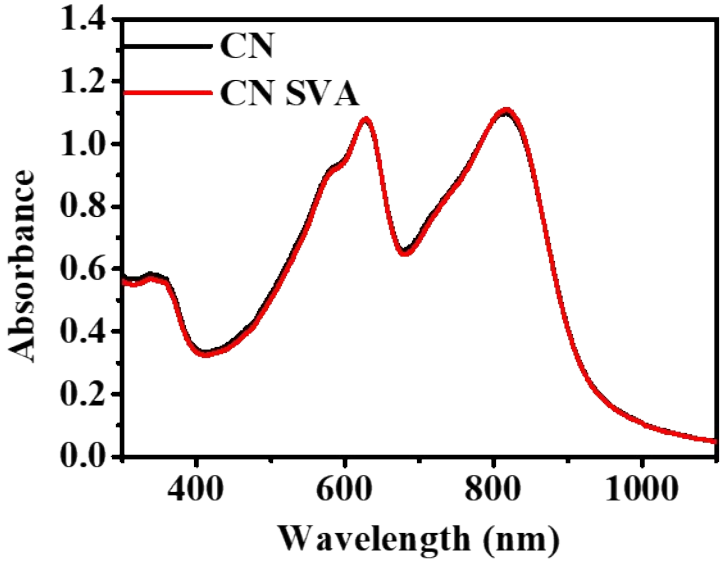

Figure S12. The absorbance of PBDB-TF:BTIC-CF3-m films with CN before and after SVA.

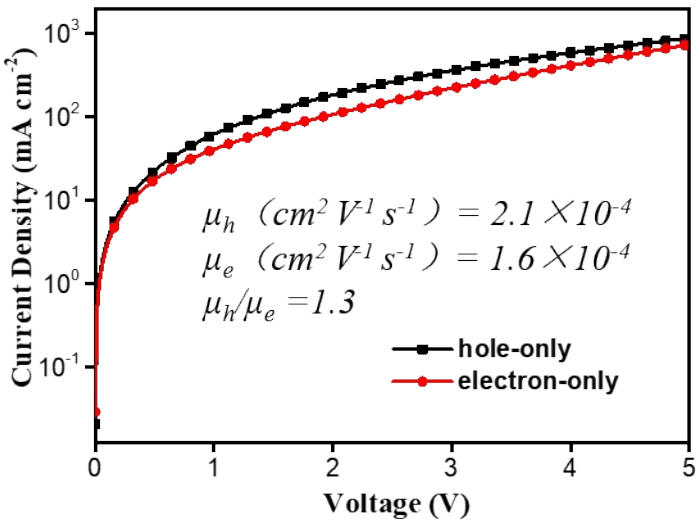

Figure S13. Dark $J-V$ curves of electron-only and hole-only devices based on PBDB-TF:BTIC-CF_3-m blend with CN after SVA.

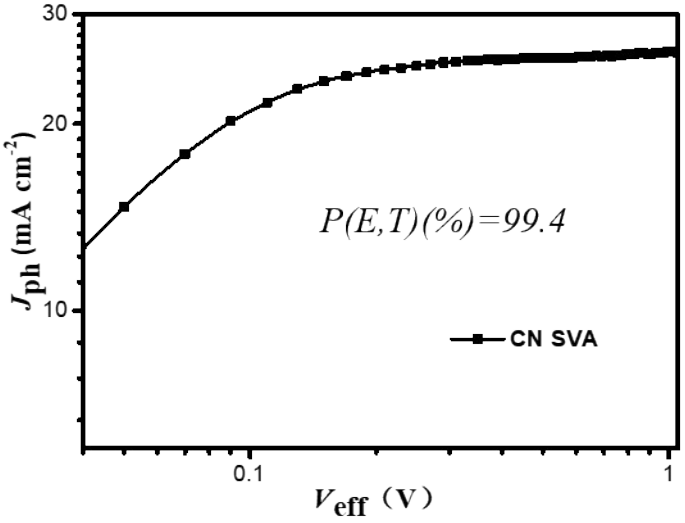

Figure S14. $J_{ph}-V_{eff}$ curves of devices based on PBDB-TF:BTIC-CF_3-m blend with CN after SVA.

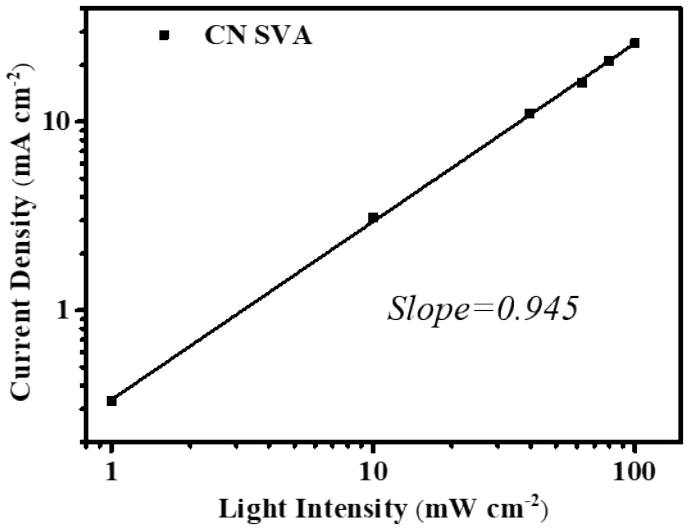

Figure S15. light intensity dependent J_{sc} of devices based on PBDB-TF:BTIC-CF_3-m blend with CN after SVA.